

Perpendicular magnetization switching by large spin—orbit torques from sputtered Bi_2Te_3

Zhenyi Zheng(郑臻益), Yue Zhang(张悦), Daoqian Zhu(朱道乾), Kun Zhang(张昆), Xueqiang Feng(冯学强), Yu He(何宇), Lei Chen(陈磊), Zhizhong Zhang(张志仲), Dijun Liu(刘迪军), Youguang Zhang(张有光), Pedram Khalili Amiri, Weisheng Zhao(赵巍胜)

Citation: Chin. Phys. B . 2020, 29(7): 078505 . **doi:** 10.1088/1674-1056/ab9439
Journal homepage: http://cpb.iphy.ac.cn; http://iopscience.iop.org/cpb

What follows is a list of articles you may be interested in

Current-induced synchronized magnetization reversal of two-body Stoner particles with dipolar interaction

Zhou-Zhou Sun(孙周洲), Yu Yang(杨玉), J Schliemann

Chin. Phys. B . 2018, 27(6): 067501 . **doi:** 10.1088/1674-1056/27/6/067501

Interfacial effect on the reverse of magnetization and ultrafast demagnetization in Co/Ni bilayers with perpendicular magnetic anisotropy

Zi-Zhao Gong(弓子召), Wei Zhang(张伟), Wei He(何为), Xiang-Qun Zhang(张向群), Yong Liu(刘永), Zhao-Hua Cheng(成昭华)

Chin. Phys. B . 2018, 27(5): 057501 . **doi:** 10.1088/1674-1056/27/5/057501

Investigation of magnetization reversal process in pinned CoFeB thin film by *in-situ* Lorentz TEM

Ke Pei(裴科), Wei-Xing Xia(夏卫星), Bao-Min Wang(王保敏), Xing-Cheng Wen(文兴成), Ping Sheng(盛萍), Jia-Ping Liu(刘家平), Xin-Cai Liu(刘新才), Run-Wei Li(李润伟)

Chin. Phys. B . 2018, 27(4): 047502 . **doi:** 10.1088/1674-1056/27/4/047502

Study of magnetization reversal and anisotropy of single crystalline ultrathin Fe/MgO (001) film by magneto-optic Kerr effect

Miao-Ling Zhang(张苗玲), Jun Ye(叶军), Rui Liu(刘锐), Shu Mi(米菽), Yong Xie(谢勇), Hao-Liang Liu(刘郝亮), Chris Van Haesendonck, Zi-Yu Chen(陈子瑜)

Chin. Phys. B . 2016, 25(4): 047503 . **doi:** 10.1088/1674-1056/25/4/047503

Micromagnetic simulation of Sm-Co/*α*-Fe/Sm-Co trilayers with various angles between easy axes and the film plane

Zhang Xi-Chao, Zhao Guo-Ping, Xia Jing, Yue Ming, Yuan Xin-Hong, Xie Lin-Hua

Chin. Phys. B . 2014, 23(9): 097504 . **doi:** 10.1088/1674-1056/23/9/097504

RAPID COMMUNICATION

Perpendicular magnetization switching by large spin–orbit torques from sputtered Bi_2Te_3*

Zhenyi Zheng(郑臻益)[1,2,3], Yue Zhang(张悦)[1,†], Daoqian Zhu(朱道乾)[1], Kun Zhang(张昆)[1], Xueqiang Feng(冯学强)[1], Yu He(何宇)[1], Lei Chen(陈磊)[1], Zhizhong Zhang(张志仲)[1,2], Dijun Liu(刘迪军)[2], Youguang Zhang(张有光)[1,2], Pedram Khalili Amiri[3], and Weisheng Zhao(赵巍胜)[1,‡]

[1] *Fert Beijing Research Institute, BDBC, School of Microelectronics, Beihang University, Beijing* 100191, *China*
[2] *School of Electronics and Information Engineering, Beihang University, Beijing* 100191, *China*
[3] *Department of Electrical and Computer Engineering, Northwestern University, Evanston, Illinois* 60208, *USA*

(Received 2 April 2020; revised manuscript received 13 May 2020; accepted manuscript online 19 May 2020)

Spin–orbit torque (SOT) effect is considered as an efficient way to switch the magnetization and can inspire various high-performance spintronic devices. Recently, topological insulators (TIs) have gained extensive attention, as they are demonstrated to maintain a large effective spin Hall angle (θ_{SH}^{eff}), even at room temperature. However, molecular beam epitaxy (MBE), as a precise deposition method, is required to guarantee favorable surface states of TIs, which hinders the prospect of TIs towards industrial application. In this paper, we demonstrate that Bi_2Te_3 films grown by magnetron sputtering can provide a notable SOT effect in the heterostructure with perpendicular magnetic anisotropy CoTb ferrimagnetic alloy. By harmonic Hall measurement, a high SOT efficiency (8.7 ± 0.9 Oe/(10^9 A/m^2)) and a large θ_{SH}^{eff} (3.3 ± 0.3) are obtained at room temperature. Besides, we also observe an ultra-low critical switching current density (9.7×10^9 A/m^2). Moreover, the low-power characteristic of the sputtered Bi_2Te_3 film is investigated by drawing a comparison with different sputtered SOT sources. Our work may provide an alternative to leverage chalcogenides as a realistic and efficient SOT source in future spintronic devices.

Keywords: spin–orbit torque, sputtered topological insulator, ferrimagnet, magnetization switching

PACS: 85.70.−w, 75.60.Jk, 75.70.Tj **DOI:** 10.1088/1674-1056/ab9439

1. Introduction

Physical mechanisms leading to controllable and stable magnetization switching are considered as the core of spintronic devices with high performance.[1–4] In recent years, researchers have found that, by applying a current through the cross-section of a non-magnetic metal (NM)/ferromagnetic metal (FM) bilayer structure, the spin–orbit interactions (SOIs) can provide strong spin torques to switch the adjacent magnetic layer via the spin–orbit torque (SOT) effect.[5–7] This method serves as a more efficient way to switch the magnetization than the spin-transfer torque (STT) effect and is expected to inspire a variety of high-speed and multifunctional spintronic devices.[8–13]

The most common spin generators in NM/FM bilayers are heavy metals (HMs), such as Ta, W, Pt, Hf, since bulk SOIs in heavier elements are much more significant.[14,15] However, the effective spin Hall angle θ_{SH}^{eff} of HM is limited, leading to a relatively high critical magnetization switching current density j_{sw} on the order of 10^{11}–10^{12} A/m.[5–7,15] Furthermore, with regard to certain high-performance bulk magnets, such as ferrimagnetic alloys,[8] Heusler alloys,[16] magnetic insulators,[17] featuring a larger thickness, j_{sw} is expected to be further increased to get over the augmenting anisotropic energy barrier. These facts seriously hinder the realization of low power consumption. Therefore, numerous studies have been conducted to investigate novel NM materials with larger θ_{SH}^{eff} such as topological insulators (TIs),[18–20] two-dimensional electron gas (2DEG),[21,22] oxidized HMs,[23,24] and so on. Among those materials, TIs (including Bi_2Te_3, Bi_2Se_3, $Bi_{0.9}Sb_{0.1}$, $(BiSb)_2Te_3$) exhibit great potential for application, thanks to the large SOTs induced by the spin–momentum locking on their surfaces at room temperature. For instance, a several-nm-thick magnetic layer can be switched by SOTs from Bi_2Se_3 or $Bi_{0.9}Sb_{0.1}$ with a j_{sw} of 10^{10} A/m,[19,20,25] while with $(BiSb)_2Te_3$, j_{sw} could even be reduced to the order of 10^9 A/m.[26] Note that all those reported TI samples are grown on single-crystal substrates with an ultra-precise growing method of molecular beam epitaxy (MBE) to form excellent topological surface states (TSS). This method is acceptable at laboratory level, but incompatible with

*Project supported by the National Natural Science Foundation of China (Grant Nos. 61971024 and 51901008), Young Elite Scientist Sponsorship Program by CAST (Grant No. 2017QNRC001), the International Mobility Project (Grant No. B16001), and National Key Technology Program of China (Grant No. 2017ZX01032101). P.K.A. acknowledges support by a grant from the National Science Foundation, Division of Electrical, Communications and Cyber Systems (NSF ECCS-1853879).

†Corresponding author. E-mail: yz@buaa.edu.cn
‡Corresponding author. E-mail: weisheng.zhao@buaa.edu.cn

© 2020 Chinese Physical Society and IOP Publishing Ltd

industrial memory or logic fabrication process. To resolve this obstacle, sputtered Bi_2Se_3 films on oxidized silicon substrate are recently reported to possess a great θ_{SH}^{eff} and can efficiently switch the adjacent ferromagnet at room temperature.[27,28] Magnetron sputtering is commonly used in semiconductor industry and therefore offers a possibility to introduce typical TI-related chalcogenides with enhanced SOT into large-scale application. Nevertheless, few similar materials are reported so far to maintain large θ_{SH}^{eff} through this method.

In this paper, we report that Bi_2Te_3 films sputtered on oxidized silicon substrate can exhibit a remarkable SOT effect. By applying harmonic Hall measurement in Bi_2Te_3/CoTb bilayer, θ_{SH}^{eff} in this system is determined as large as 3.3 ± 0.3 at room temperature. Then, current-induced switching of a 6-nm-thick perpendicular magnetic anisotropy (PMA) CoTb ferrimagnetic alloy is also realized in the mentioned structure. Compared with traditional HMs, j_{sw} as well as the power consumption to switch the magnetic layer can be reduced by more than one order.

2. Method

The samples in our work are deposited on thermally oxidized Si substrates using DC or RF magnetron sputtering under a base pressure better than 2×10^{-8} Torr. We first deposited a series of substrate/MgO (2 nm)/Bi_2Te_3 (t nm)/MgO (1 nm) stacks with t varying from 5 nm to 40 nm for the four-point resistivity measurements. Figure 1(a) shows that the resistivity of the sputtered Bi_2Te_3 has a downward trend versus its thickness t. This trend is similar to those in previously reported TI materials[20] and can be explained by the combined effect of surface conduct and bulk conduct properties in Bi_2Te_3.[29] To guarantee a relatively good θ_{SH}^{eff} as well as enough passing current through the cross-section, 8-nm-thick Bi_2Te_3 layer with a resistivity of 3011 μΩ·cm is chosen for the SOT experiments in our work. This Bi_2Te_3 layer should have a polycrystalline structure, and the roughness characterized by atomic force microscope (AFM) is shown in the inset of Fig. 1(a). The root mean square value of the surface roughness is 0.35 nm, which is smooth enough for the following heterostructure deposition.

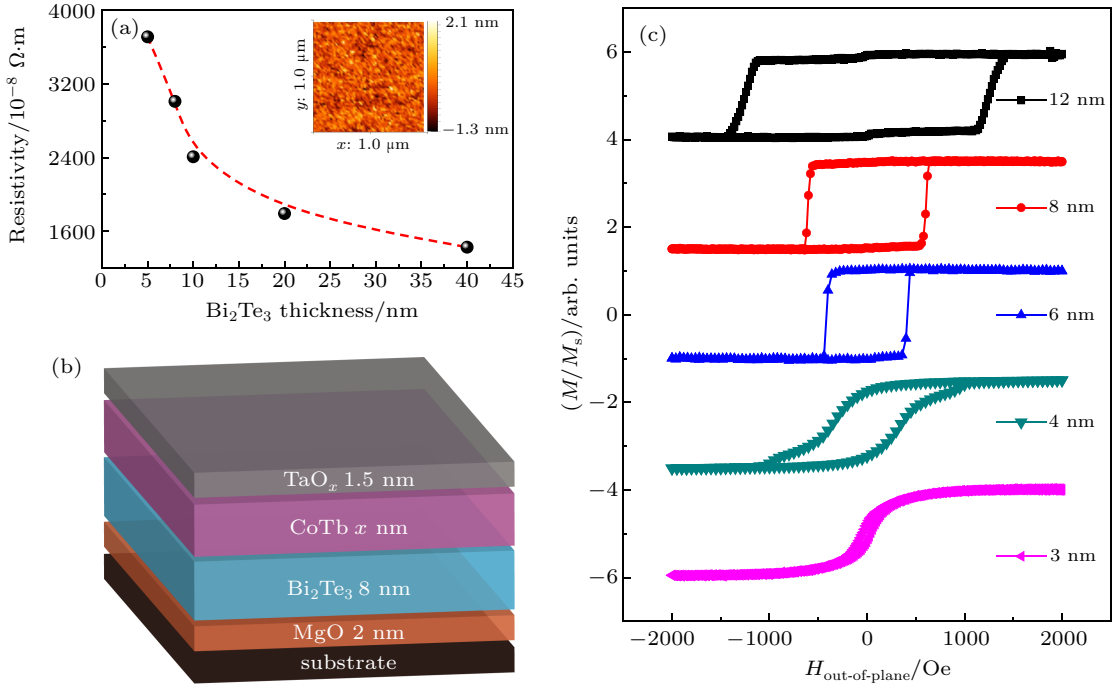


Fig. 1. (a) Thickness-dependent resistivity change measured by four-point method in MgO/Bi_2Te_3/MgO trilayers. Inset is an AFM image of Bi_2Te_3 (8 nm) sample. (b) Stack schematic of the investigated Bi_2Te_3/CoTb heterostructure. (c) Dependence of the magnetization direction of CoTb layer on x. When x is in the range of 6–8 nm, CoTb layers show excellent PMA properties.

In addition, a ferrimagnetic rare-earth-transition–metal alloy CoTb, in which Co and Tb sub-lattices are coupled antiferromagnetically, is used as the adjacent magnetic layer for two reasons: 1) CoTb alloy possesses robust bulk PMA within a large thickness range, and bulk PMA magnets present better switching performance and thermal stability in real device applications;[19,30] 2) CoTb alloy has a relatively high resistivity (206 μΩ·cm), allowing more current to pass through the Bi_2Te_3 layer. Here, CoTb is deposited by the co-sputtering of Co and Tb targets. By tuning the chemical composition or temperature, CoTb could approach angular momentum compensation point or magnetization compensation point, and exhibits plenty of charming magnetic properties.[30–32] However, few evidences yet support that CoTb approaching compensation point could contribute to increase θ_{SH}^{eff} in the whole system. Therefore, we use a Co-rich chemical composition, i.e., $Co_{0.83}Tb_{0.17}$, throughout our whole work, which is estimated by the independent deposition speed of Co and Tb. As

shown in Fig. 1(b), a series of substrate/MgO (2 nm)/Bi_2Te_3 (8 nm)/CoTb (x nm)/Ta (1.5 nm) stacks are deposited. It can be found that the capping Ta layers are fully oxidized and not involved in the SOT switching process.[33] Vibration sample magnetometry is utilized to determine the magnetic anisotropies of all the samples. As illustrated in Fig. 1(c), when x ranges from 3 nm to 12 nm, the magnetization direction of the CoTb varies from in-plane to out-of-plane, and tends to go slightly back to the in-plane state when x reaches 12 nm.

For electrical measurements, we choose the 6-nm-thick CoTb sample, since it possesses good PMA when the magnetic layer remains relatively thin. The net magnetization M_s of this 6-nm-thick CoTb layer is 215 emu/cc. By typical lithography and ion beam etching, the sample is fabricated into 5-μm-width Hall bar device. Keithley 6221 current source and 2182 voltage-meter are used to implement AHE and SOT switching experiments. To measure the SOT efficiency, harmonics Hall measurement is then implemented by injecting an AC current of 133.33 Hz along x axis. Two SR830 lock-in amplifiers are used to detect the harmonic signals.

3. Result and discussion

Figure 2(a) shows the fabricated device with gold electrodes and the basic electrical measurement schematic. The anomalous Hall effect (AHE) resistance versus the applied out-of-plane magnetic field is plotted in Fig. 2(b). Squared loop and similar coercive field confirm that the stack maintains its as-deposited magnetic properties. Figure 2(c) plots the curves of the first and the second harmonic voltages, i.e., $R_{1\omega}$ and $R_{x(y),2\omega}$ versus the in-plane magnetic field $H_{x(y)}$. A ratio coefficient $B_{x(y)}$ could be firstly calculated with the respective curvature of $R_{1\omega}$ and the slope of $V_{x(y),2\omega}$[34,35]

$$B_{x(y)} = \left(\frac{\partial R_{x(y),2\omega}}{\partial H_{x(y)}}\right) \times \left(\frac{\partial^2 R_{1\omega}}{\partial H_{x(y)}^2}\right)^{-1}. \quad (1)$$

Then, the damping-like H_{DL} and field-like effective field H_{FL} can be determined by the following expression:[34,35]

$$H_{DL(FL)} = -2 \times \frac{B_{x(y)} \pm 2\xi B_{y(x)}}{1 - 4\xi^2}, \quad (2)$$

where ξ is the ratio of planar Hall resistance R_{PHE} and AHE resistance R_{AHE}. The measured R_{PHE} in our samples is about 0.06 Ω, which is much smaller than R_{AHE} and thus can be negligible. In this occasion, $H_{DL(FL)} \approx -2B_{x(y)}$. Moreover, it also should be noticed that $R_{x,2\omega}$ induced by the field along x axis is much larger than $R_{y,2\omega}$ induced by the field along y axis, even if $R_{y,2\omega}$ is amplified by 3 times in Fig. 2(c). This phenomenon indicates that the induced H_{FL} is negligible compared to the induced H_{DL}; for this reason, we concentrate on the damping-like SOT effect in the following discussion.

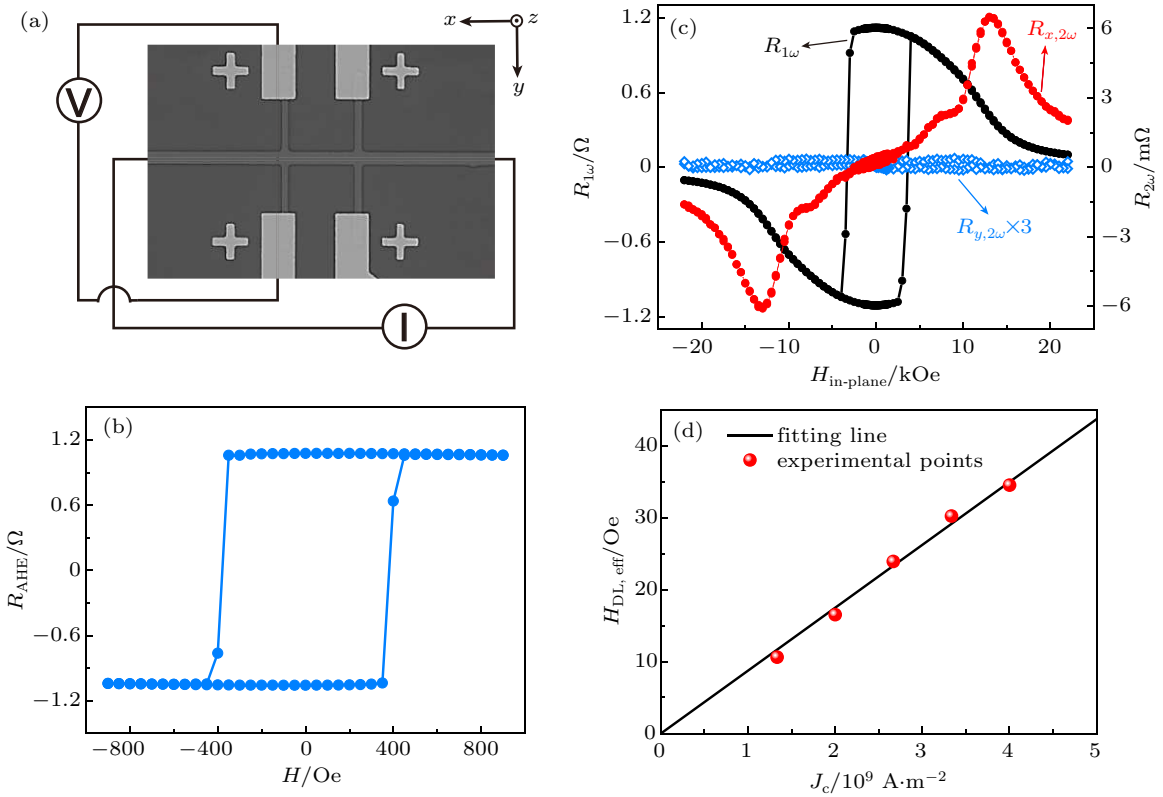


Fig. 2. (a) Image of 5-μm-width Hall bar device with electrical measurement setup. (b) Anomalous Hall resistance curve of Bi_2Te_3 (8 nm)/CoTb (6 nm) sample. (c) Harmonics resistance curve with applied in-plane magnetic field. H_x-induced damping-like signal (red points) is much larger than H_y-induced field-like signals (blue circles, amplified by 3 times). (d) Effective damping-like field as a linear function of current density in Bi_2Te_3 layer.

Figure 2(d) shows the calculated H_{DL} as a function of applied charge current density j_c in the Bi_2Te_3 layer. Here, j_c is calculated by a parallel circuit model of Bi_2Te_3/CoTb bilayer, which can be written as

$$j_c = \frac{\rho_{CoTb}}{\rho_{Bi_2Te_3} t_{CoTb} + \rho_{CoTb} t_{Bi_2Te_3}} \frac{I}{w_{HallBar} t_{Bi_2Te_3}}, \quad (3)$$

where ρ_{CoTb}, $\rho_{Bi_2Te_3}$, t_{CoTb}, $t_{Bi_2Te_3}$, $w_{HallBar}$ and I represent the resistivity of CoTb, resistivity of Bi_2Te_3, thickness of CoTb, thickness of Bi_2Te_3, width of Hall bar, and injected current, respectively. H_{DL} augments linearly with the increasing current density, revealing that Joule heating effect is negligible in the measured current density range.[32] In the investigated Bi_2Te_3/CoTb sample, the determined current-induced SOT efficiency χ (defined by H_{DL}/j_c) is 8.7 ± 0.9 Oe/(10^9 A/m^2). Although the applied CoTb is far from its magnetic compensation point, the obtained value is surprisingly high. For comparison, χ in W/CoTb/AlO_x structure in our previous work is about 0.4 ± 0.04 Oe/(10^9 A/m^2),[8] while χ in a conventional Ta/CoFeB/MgO structure is 0.2–0.9 Oe/(10^9 A/m^2).[36,37] This outstanding χ indicates that strong SOTs are expected in the sputtered Bi_2Te_3 layer. We also calculate the θ_{SH}^{eff} in this system by the following expression:[30–33]

$$\theta_{SH}^{eff} = \frac{2e}{\hbar} \frac{M_s t_{CoTb} H_{eff}}{J_c}, \quad (4)$$

where t_{CoTb} is thickness of CoTb. The obtained $\theta_{SH}^{eff} \approx 3.3 \pm 0.3$, which exceeds 100% and is competitive with the results in MBE-grown TIs.[18–20] In addition, it is worth mentioning that there might be spin loss at the interface between Bi_2Te_3 and CoTb. Given this fact, even a larger intrinsic spin Hall angle could be expected in our sputtered Bi_2Te_3 films.

Current-induced magnetization switching at room temperature is demonstrated as well and plotted in Figs. 3(a) and 3(d). Here, a series of 0.1-ms-width current pulses are applied to switch the magnet, while a 400 Oe in-plane magnetic field is used to break the magnetization precession symmetry. The j_{sw} to switch 6-nm-thick CoTb is about 9.7×10^9 A/m^2. This value is one or two orders lower than that in typical HM-based heterostructure,[5–8] confirming again the existence of strong SOTs in the sputtered Bi_2Te_3. When the direction of the applied in-plane field is reversed, the switching polarity of the curve changes as expected in the theoretical SOT switching framework. We also notice that the variation of SOT-driven R_{AHE} (~ 1.6 Ω) is smaller than that of magnetic-field-driven R_{AHE} (~ 2.1 Ω), revealing a partial switching phenomenon (76% magnetization). This difference is also observed in previous switching results with MBE-grown TIs and can be explained by the Joule-heating-caused demagnetization in CoTb layer.[26] We are convinced that reducing shunting current in CoTb layer by reasonable device design could efficiently eliminate the problem.

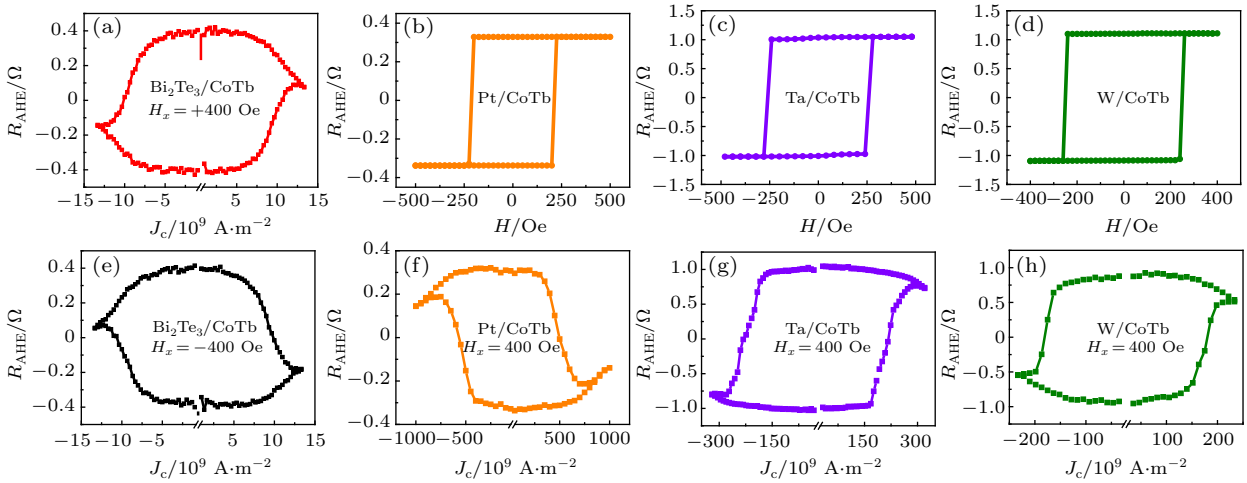


Fig. 3. Current-induced switching curves of Bi_2Te_3/CoTb under an in-plane magnetic field $H_x = 400$ Oe (a) and -400 Oe (e). (b)–(c) The AHE curves of Pt/CoTb, Ta/CoTb, and W/CoTb samples, respectively. (f)–(h) The current-induced switching curves of Pt/CoTb, Ta/CoTb, and W/CoTb samples under $H_x = 400$ Oe. The different switching polarities reveal different spin Hall angle signs.

To better evaluate the SOT performance of the sputtered Bi_2Te_3 sample, some control samples based on conventional sputtered SOT sources (Pt, Ta, W) are also studied with a stack structure of HM (5 nm)/CoTb (4 nm). While maintaining the same chemical composition and M_s, the thickness of CoTb is reduced in these samples, since SOTs originating from common HMs can hardly switch magnets with large thickness. As shown in Figs. 3(b)–3(d), all the control samples have squared R_{AHE} loops versus perpendicular magnetic field, indicating that they possess good PMA properties. Besides, because of the different shunting effects of Bi_2Te_3, Pt, Ta, and W, R_{AHE} in the four samples are not consistent. Figures 3(f)–3(h) illustrate the current-induced magnetization switching curves of Pt/CoTb, Ta/CoTb, and W/CoTb samples. In these experiments, the applied in-plane magnetic field is fixed to +400 Oe to guarantee a more reasonable comparison. We observe similar R_{AHE} in current-induced switching and field-induced switching for each sample, revealing that

the aforementioned partial switching phenomenon barely exists in HM based samples. Regarding the calculation of current density, the resistivity of Pt, Ta, and W is measured to be 27 μΩ·cm, 112 μΩ·cm, and 151 μΩ·cm, respectively. We find that the values of j_{sw} to switch 4-nm-CoTb for Pt, Ta, and W are approximately 5.5×10^{11} A/m^2, 2.3×10^{11} A/m^2, and 1.7×10^{11} A/m^2. All those critical current densities are consistent with previously reported values[5,7,8] and are obviously much larger than those in our Bi_2Te_3/CoTb system, although CoTb in Bi_2Te_3 based sample is even thicker, i.e., 6 nm. Note that, under an in-plane field with fixed direction, the switching polarity in Bi_2Te_3 sample is in line with that in Ta or W samples, which is opposite to that in Pt sample. This SOT polarity characteristic indicates that our sputtered Bi_2Te_3 possesses the same spin Hall angle sign as Ta and W, but is opposite to Pt. Nevertheless, this phenomenon is in contradiction with SOTs in previous-reported Bi-based materials: both MBE-grown TIs and sputtered Bi_2Se_3 films are demonstrated to have the same sign as Pt.[19,20,25–27] The origin of this difference will be discussed subsequently. In our work, values of θ_{SH}^{eff} of Pt, Ta, and W in Fig. 4(a) are determined as 0.07 ± 0.007, 0.14 ± 0.01, and 0.18 ± 0.02, through previously mentioned harmonic measurement and Eq. (4). In accordance with the varying j_{sw} values in those SOT materials, these calculated values are quite reliable and accepted in our following discussion.

Essentially, improving the magnetization switching energy efficiency is the eventual goal of obtaining higher θ_{SH}^{eff}. Considering that the resistivity of our sputtered Bi_2Te_3 is similar to that of MBE-grown TIs and can be dozens, even hundreds of times higher than that of conventional HMs, we think that it is significant to figure out whether the sputtered Bi_2Te_3 indeed offers energy superiority by calculating the switching power consumption P. Basically, P to switch the magnetization of CoTb per unit volume with different SOT sources can be analyzed by a heat dissipation formula[27]

$$P \propto \rho_{SOTsource}\cdot j_{sw}^2, \tag{5}$$

where $\rho_{SOTsource}$ is the resistivity of the certain SOT source material. As shown by orange bars in Fig. 4(b), the power consumption for Bi_2Te_3 in this model is 3.7%, 3.2%, and 3.9% of that for Pt, Ta, and W, indicating that sputtered Bi_2Te_3 is a low-power SOT source. Furthermore, since $j_{sw}\propto\theta_{SH}^{eff-1}$ theoretically, another formula is considered as well to confirm the results[19]

$$P \propto \rho_{SOTsource}\cdot \theta_{SH}^{eff-2}. \tag{6}$$

Black bars in Fig. 4(b) reveal that, although the calculated power of Pt, Ta, W with Eq. (5) varies in a possible range compared to those values with Eq. (4), the sputtered Bi_2Te_3 material still shows the best energy efficiency performance (2.8%, 3.5%, and 4.3% of that for Pt, Ta, and W).

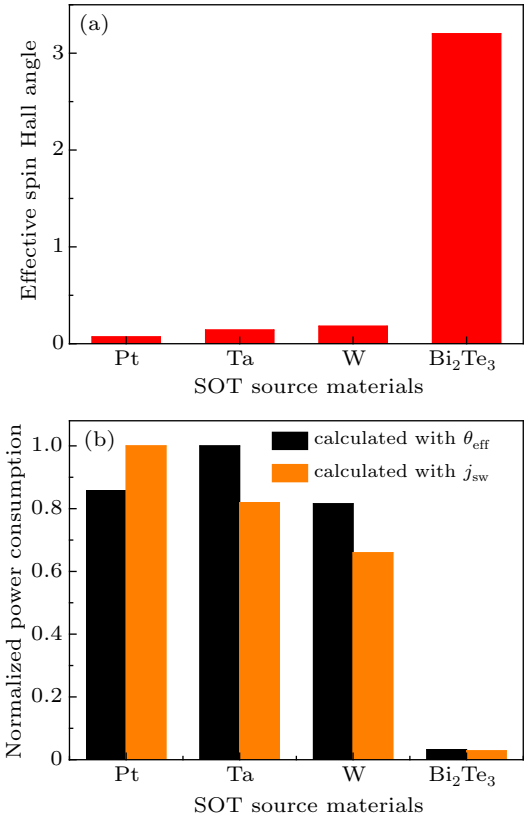


Fig. 4. (a) Effective spin Hall angles of sputtered Pt, Ta, W, and Bi_2Te_3. (b) Normalized power consumption to switch the magnetization of CoTb per unit volume by different SOT source materials. The black bars and orange bars correspond respectively to the calculation formulas related to θ_{SH}^{eff} and j_{sw}.

Last but not least, we will discuss about the origin of the strong SOTs in the sputtered Bi_2Te_3 films. In MBE-grown TIs, SOTs basically come from the spin–momentum locking in TSS. Thus, great surface quality is the basic precondition to gain large θ_{SH}^{eff}. However, good TSS definitely will not appear in the deposited Bi_2Te_3 films, since magnetron sputtering is a rapid and rough growing method. Generally, there are two possible reasons to answer this question: 1) sputtered Bi chalcogenides could possibly possess nanoscale grain structure. Some *ab initio* calculation results suggest that this reduced dimensionality may contribute to the non-equilibrium spin accumulation driven by intraband Edelstein effect.[27] 2) It is also possible that remarkable SOIs already exist in the sputtered Bi_2Te_3 films with relatively high resistivity and heavy elements. To further analyze the possible origin, an important point is that, the observed spin Hall angle sign of our sputtered Bi_2Te_3 films is opposite to that in MBE-grown TIs (same as Pt). Another recent work also reports a similar result: sputtered W_xTe_{1-x} films possess opposite spin Hall angle sign to WTe_2 single crystals.[38–40] However, for related Se-based material, the sputtered Bi_2Se_3 films have the same spin Hall angle to the MBE-grown Bi_2Se_3.[27,28] Those evidences indicate that sputtered Te-based films probably exhibit different SOT mechanisms to sputtered Se-based films, although they both belong to the Bi chalcogenide class. Be-

sides, the opposite spin Hall angle signs of sputtered Bi_2Te_3 and MBE-grown Bi_2Te_3 also exclude the possibility of major origin from TSS. Therefore, considering that both sputtered Te-based materials[38] and Bi-based chalcogenides[27] are reported to have obvious thickness-dependent spin Hall angle, the second reason attached to intrinsic bulk spin Hall effect is more convincing from our perspective.

4. Conclusion

In summary, we investigate SOTs in Bi_2Te_3 films grown by an industry-compatible deposition method magnetron sputtering. A high SOT efficiency χ (8.7 ± 0.9 Oe/(10^9 A/m^2)) and a remarkable θ_{SH}^{eff} (3.3 ± 0.3) are obtained in Bi_2Te_3/CoTb heterostructure as shown by harmonic Hall measurement. In addition, an ultra-low current switching current density (9.7×10^9 A/m^2 to switch 6-nm-thick PMA CoTb) is achieved as well. Compared with other sputtered SOT sources, the sputtered Bi_2Te_3 in our work shows much higher energy efficiency, indicating that it is a promising candidate in future SOT spintronic devices. Our work may also provide an alternative route to introduce more laboratory-level high-performance chalcogenides in industry-level spintronic applications.

References

[1] Slonczewski J C 1996 *J. Magn. Magn. Mater.* **159** L1

[2] Wadley P, Howells B, Železný J, Andrews C, Hills V, Campion R P, Novák V, Olejník K, Maccherozzi F, Dhesi S S, Martin S Y, Wagner T, Wunderlich J, Freimuth F, Mokrousov Y, Kuneš J, Chauhan J S, Grzybowski M J, Rushforth A W, Edmonds K W, Gallagher B L and Jungwirth T 2016 *Science* **351** 587

[3] Chen X, Zhou X, Cheng R, Song C, Zhang J, Wu Y, Ba Y, Li H, Sun Y, You Y, Zhao Y and Pan F 2019 *Nat. Mater.* **18** 931

[4] Yang T, Kimura T and Otani Y 2008 *Nat. Phys.* **4** 851

[5] Liu L, Pai C F, Li Y, Tseng H W, Ralph D C and Buhrman R A 2012 *Science* **336** 555

[6] Miron I M, Garello K, Gaudin G, Zermatten P G, Costache M V, Auffret S, Bandiera S, Rodmacq B, Schuhl A and Gambardella P 2011 *Nature* **476** 189

[7] Yu G, Upadhyaya P, Fan Y, Alzate J G, Jiang W, Wong K L, Takei S, Bender S A, Chang L T, Jiang Y, Lang M, Tang J, Wang Y, Tserkovnyak Y, Amiri P K and Wang K L 2014 *Nat. Nanotechnol.* **9** 548

[8] Zheng Z, Zhang Y, Feng X, Zhang K, Nan J, Zhang Z, Wang G, Wang J, Lei N, Liu D, Zhang Y G and Zhao W S 2019 *Phys. Rev. Appl.* **12** 044032

[9] Sato N, Xue F, White R M, Bi C and Wang S X 2018 *Nat. Electron.* **1** 508

[10] Zhang Z, Zhu Y, Zhang Y, Zhang K, Nan J, Zheng Z, Zhang Y G and Zhao W S 2019 *IEEE Electron. Device. Lett.* **40** 1984

[11] Zhang K, Zhang Y, Zhang Z, Zheng Z, Wang G, Zhang Y G, Liu Q, Yan S and Zhao W S 2019 *Adv. Electron. Mater.* **5** 1800812

[12] Wang M, Cai W, Zhu D, Wang Z, Kan J, Zhao Z, Cao K, Wang Z, Zhang Y, Zhang T, Park C, Wang J P, Fert A and Zhao W S 2018 *Nat. Electron.* **1** 582

[13] Zheng C, Chen H, Zhang X, Zhang Z and Liu Y 2019 *Chin. Phys. B* **28** 037503

[14] Feng X, Zhang Q, Zhang H, Zhang Y, Zhong R, Lu B, Cao J and Fan X 2019 *Chin. Phys. B* **28** 107105

[15] Ramaswamy R, Qiu X, Dutta T, Pollard S D and Yang H 2016 *Appl. Phys. Lett.* **108** 202406

[16] Finley J, Lee C H, Huang P Y and Liu L 2019 *Adv. Mater.* **31** 1805361

[17] Li P, Liu T, Chang H, Kalitsov A, Zhang W, Csaba G, Li W, Richardson D, DeMann A, Rimal G, Dey H, Jiang J S, Porod W, Field S, Tang J, Marconi M C, Hoffmann A, Mryasov O and Wu M 2016 *Nat. Commun.* **7** 12688

[18] Mellnik A R, Lee J S, Richardella A, Grab J L, Mintun P J, Fischer M H, Vaezi A, Manchon A, Kim E A, Samarth N and Ralph D C 2014 *Nature* **511** 449

[19] Han J, Richardella A, Siddiqui S A, Finley J, Samarth N and Liu L 2017 *Phys. Rev. Lett.* **119** 077702

[20] Wang Y, Zhu D, Wu Y, Yang Y, Yu J, Ramaswamy R, Mishra R, Shi S, Elyasi M, Teo K L, Wu Y and Yang H 2017 *Nat. Commun.* **8** 1

[21] Yang H, Zhang B, Zhang X, Yan X, Cai W, Zhao Y, Sun J, Wang K L, Zhu D and Zhao W S 2019 *Phys. Rev. Appl.* **12** 034004

[22] Ohtomo A and Hwang H Y 2004 *Nature* **427** 423

[23] Kageyama Y, Tazaki Y, An H, Harumoto T, Gao T, Shi J and Ando K 2019 *Sci. Adv.* **5** eaax4278

[24] An H, Ohno T, Kanno Y, Kageyama Y, Monnai Y, Maki H and Ando K 2018 *Sci. Adv.* **4** eaar2250

[25] Khang N H D, Ueda Y and Hai P N 2018 *Nat. Mater.* **17** 808

[26] Wu H, Xu Y, Deng P, Pan Q, Razavi S A, Wong K, Huang L, Dai B, Shao Q, Yu G, Han X, Sánchez J C R, Mangin S and Wang K L 2019 *Adv. Mater.* **31** 1901681

[27] Mahendra D C, Grassi R, Chen J, Jamali M, Hickey D R, Zhang D, Zhao Z, Li H, Quarterman P, Lv Y, Li M, Manchon A, Mkhoyan K A, Low T and Wang J P 2018 *Nat. Mater* **17** 800

[28] Zhang X, Cui B, Mao J, Yun J, Yan Z, Chang M, Zuo Y and Xi L 2020 *Phys. Status Solidi-Rapid Res. Lett.* **14** 2000033

[29] Sourabh, B, Rajeev and K P 2014 *AIP Adv.* **4** 017135

[30] Finley J and Liu L 2016 *Phys. Rev. Appl.* **6** 054001

[31] Ueda K, Mann M, de Brouwer P W P, Bono D and Beach G S D 2017 *Phys. Rev. B* **96** 064410

[32] Je S G, Sánchez J C R, Pham T H, Vallobra P, Malinowski G, Lacour D, Fache T, Cyrille M C, Kim D Y, Choe S B, Belmeguenai M, Hehn M, Mangin S, Gaudin G and Boulle O 2018 *Appl. Phys. Lett.* **112** 062401

[33] Woo S, Mann M, Tan A J, Caretta L and Beach G S D 2014 *Appl. Phys. Lett.* **105** 212404

[34] Hayashi M, Kim J, Yamanouchi M and Ohno H 2014 *Phys. Rev. B* **89** 144425

[35] Garello K, Miron I M, Avci C O, Freimuth F, Mokrousov Y, Blügel S, Auffret S, Boulle O, Gaudin G and Gambardella P 2013 *Nat. Nanotechnol.* **8** 587

[36] Zhang S, Su Y, Li X, Li R, Tian W, Hong J and You L 2019 *Appl. Phys. Lett.* **114** 042401

[37] Cao J, Chen Y, Jin T, Gan W, Wang Y, Zheng Y, Lv H, Cardoso S, Wei D and Lew W S 2018 *Sci. Rep.* **8** 1355

[38] Li X, Li P, Hou V D H, Mahendra D C, Nien C H, Xue F, Yi D, Bi C, Lee C M, Lin S J, Tsai W, Suzuki Y and Wang S X 2020 arXiv:2001.04054[cond-mat.mes-hall]

[39] Shi S, Liang S, Zhu Z, Cai K, Pollard S D, Wang Y, Wang J, Wang Q, He P, Yu J, Eda G, Liang G and Yang H 2019 *Nat. Nanotechnol.* **14** 945

[40] Li P, Wu W, Wen Y, Zhang C, Zhang J, Zhang S, Yu Z, Yang S A, Manchon A and Zhang X 2018 *Nat. Commun.* **9** 3990